Original Article

Sclerostin aggravates cardiac remodeling after myocardial infarction by inhibition of Wnt/β-catenin signaling pathway

Shuxin Zheng[1#]^, Jinyi Wei[1#], Peipei Chen[1,2], Fangliang Chen[1], Guang Yang[1,2]

[1]Second Clinical College, Guangzhou University of Chinese Medicine, Guangzhou, China; [2]Department of Critical Care Medicine, Guangdong Provincial Hospital of Chinese Medicine, Guangzhou, China

Contributions: (I) Conception and design: S Zheng, J Wei; (II) Administrative support: G Yang, P Chen; (III) Provision of study materials or patients: F Chen; (IV) Collection and assembly of data: S Zheng, J Wei, F Chen; (V) Data analysis and interpretation: P Chen; (VI) Manuscript writing: All authors; (VII) Final approval of manuscript: All authors.

[#]These authors contributed equally to this work.

Correspondence to: Professor Guang Yang. Second Clinical College, Guangzhou University of Chinese Medicine, Dade Road, Guangzhou 510120, China. Email: yg_1918@163.com.

Background: The serum levels of sclerostin (SOST) are significant elevated in patients with pathological cardiac remodeling after myocardial infarction (MI). However, the mechanisms of SOST in cardiac remodeling remain largely uncharacterized.

Methods: Collecting patients with MI who presented with or without left ventricular (LV) remodeling, we investigated differences in SOST expression. The influence of overexpression and silenced of SOST on the angiogenesis of cardiac microvascular endothelial cells (CMECs) was explored through *in vitro* experiments, and the impact of SOST on Wnt signaling marker proteins was examined by quantitative reverse transcription-polymerase chain reaction (qRT-PCR) and Western blot. Finally, we observed the effects of SOST on cardiac function and morphology in mice MI model, and verified the role of the Wnt signaling marker proteins *in vivo*.

Results: Serum SOST was significantly increased in patients with cardiac remodeling. Increased SOST expression was also observed in the infarcted hearts of C57BL/6 mice that underwent ligation of the left anterior descending branch of the coronary artery to induce MI. Furthermore, loss and gain of function experiments were conducted to investigate the role of SOST in post-infarct cardiac remodeling *in vivo* and *in vitro*. Overexpression of SOST promoted the proliferation and migration of cardiac fibroblasts (CFs), and inhibited angiogenesis of CMECs. In addition, overexpressing SOST in mice significantly deteriorated the post-infarct cardiac remodeling, as shown by the increased LV end systolic and end diastolic dimensions, decreased ejection fraction, and increased myocyte cross-section area and myocardial fibrosis. However, suppressing SOST expression showed the opposite results. The expression of Wnt signaling marker proteins was inhibited after overexpression of SOST, and enhanced after suppression of SOST *in vivo* and *in vitro*, suggesting involvement of the Wnt signaling pathway.

Conclusions: The present study demonstrated that SOST aggravates post-infarct pathological myocardial remodeling by inhibiting angiogenesis of CMECs while promoting the proliferation of CFs, and this may be mediated by the Wnt signaling pathway. These results suggested that SOST might act as a biomarker to predict detrimental postinfarct cardiac remodeling, and may be a potential therapeutic target for the treatment of MI.

Keywords: Sclerostin (SOST); cardiac remodeling; myocardial infarction (MI); Wnt/β-catenin signaling

^ ORCID: 0000-0002-4272-1856.

Submitted Mar 17, 2022. Accepted for publication May 13, 2022.
doi: 10.21037/jtd-22-473
View this article at: https://dx.doi.org/10.21037/jtd-22-473

Introduction

Myocardial infarction (MI) is the ischemia-hypoxic necrosis of the myocardium which is caused by the drastic reduction or interruption of the blood flow in the coronary artery (1). It is one of the leading causes of death and disability from cardiovascular disease. Severe pathophysiological changes occur in cardiac tissues after MI, including inflammation, apoptosis, myocardial hypertrophy, and fibrosis, leading to cardiac remodeling, heart failure, and eventually, cardiac death (2). In recent years, with the widespread development of thrombolysis, interventional heart surgery, drug therapy, and lifestyle changes, the mortality rate of MI has decreased dramatically, and the prognosis has improved significantly. Although some patients recover after successful reperfusion, many will experience cardiac remodeling which eventually leads to heart failure (3).

Cardiac remodeling is characterized by progressive left ventricular (LV) dilation and depressed LV function, induced by multiple regulatory mechanisms of the heart and the whole body after MI. This progressive pathological process includes inflammatory cell infiltration, morphological structural changes in the cardiomyocytes, and release of intercellular substances caused by cytokine secretion. The molecular mechanisms of cardiac remodeling after MI is complex and involves multiple factors and molecules, such as cytokines, genes, transcription factors, noncoding RNAs, and epigenetic regulation (4). With advancement in technology, there is now growing evidence that the expression of these factors and their function are involved in maladaptive cardiac remodeling. For example, ablation of the interleukin 33 (*IL-33*) gene exacerbates myocardial remodeling in mice with heart failure induced by mechanical stress (5).Transfer and upregulation of microRNA-543 promotes cardiac microvascular endothelial cells (CMECs) angiogenesis after MI, and this process can reduce scarring and adverse LV remodeling (6). A recent report showed that DNA methylation reprogramed cardiac metabolic gene expression in end-stage human heart failure (7). Moreover, several factors have been shown to be potential molecular markers of cardiac remodeling. However, the mechanisms of action of these factors in cardiac remodeling after MI remain unclear. Therefore, it is crucial to identify and understand the novel mechanisms involved in cardiac remodeling after MI, so as to develop innovative therapies.

Sclerostin (SOST) is produced by osteocytes, which regulate bone formation (8). An increasing number of studies have shown that SOST may participate in various diseases, such as ankylosis spondylitis, type 2 diabetes, and atherosclerotic plaques (9-11). Furthermore, circulating levels of SOST are considered to be associated with cardiovascular mortality (12-15). A recent meta-analysis of clinical trials and human genetics demonstrated that SOST genetic variants were associated with a lower risk of fractures and osteoporosis, and a higher risk of MI and/or coronary revascularization and major adverse cardiovascular events (16). Indeed, our previous proteomics study revealed that the expression of SOST was significantly increased in MI patients who developed malignant cardiac remodeling compared to MI patients without cardiac remodeling and healthy participants (17). SOST is a natural inhibitor of the Wnt pathway, and studies have shown that inhibition of the Wnt/β-catenin pathway promotes apoptosis, impairs ability of regeneration, and leads to cardiac dysfunction (18,19). However, the precise role of SOST in the failing heart remains to be fully elucidated. Therefore, this present study was designed to investigate the biological effects and mechanisms of SOST in the pathophysiological process of cardiac remodeling. Using *in vivo* and *in vitro* models, this study demonstrated that SOST deteriorated post-MI cardiac remodeling, decreased angiogenesis of CMECs and capillary density, increased the proliferation of cardiac fibroblasts (CFs) and LV fibrosis, and inhibited Wnt/β-catenin signaling. We present the following article in accordance with the ARRIVE reporting checklist (available at https://jtd.amegroups.com/article/view/10.21037/jtd-22-473/rc).

Methods

Clinical sample and ethical statement

Patients with MI who presented with or without LV remodeling diagnosed in Guangdong Provincial Hospital of Chinese Medicine from October 2020 to October 2021 were enrolled in this study. Healthy participants were recruited as the control group. All participants signed the

Table 1 Primer sequences of genes

Name	Primer
Wnt1	F: 5'-CGATGGTGGGGTATTGTGAAC-3'
	R: 5'-CCGGATTTTGGCGTATCAGAC-3'
APC	F: 5'-AAAATGTCCCTCCGTTCTTATGG-3'
	R: 5'-CTGAAGTTGAGCGTAATACCAGT-3'
GSK3β	F: 5'-GGCAGCATGAAAGTTAGCAGA-3'
	R: 5'-GGCGACCAGTTCTCCTGAATC-3'
β-catenin	F: 5'-AAAGCGGCTGTTAGTCACTGG-3'
	R: 5'-CGAGTCATTGCATACTGTCCAT-3'
GAPDH	F: 5'-ACAACTTTGGTATCGTGGAAGG-3'
	R: 5'-GCCATCACGCCACAGTTTC-3'
SOST shRNA	5'-GTGGCAGGCGTTCAAGAATGA-3'

R, reverse; F, forward; SOST, sclerostin; APC, adenomatous polyposis coli; GSK3β, glycogen synthase kinase 3β; GAPDH, glyceraldehyde 3-phosphate dehydrogenase; sh, short hairpin.

project informed consent forms. The Ethics Committee of Guangdong Provincial Hospital of Chinese Medicine approved this project (Z2017-080-01). The study was conducted in accordance with the Declaration of Helsinki (as revised in 2013). The serum samples were separated and stored by Biological Resource Center of Guangdong Provincial Hospital of Chinese Medicine. The person collecting the experimental measurements or conducting the analyses was blinded to the treatments for each sample. A protocol was prepared before the study without registration.

Cell culture and transfection

Human cardiac microvascular endothelial cells (CMECs) and human CFs were purchased from the American Type Culture Collection (ATCC, Bethesda, MD, USA). CMECs and CFs were cultured at 37 ℃ in a 5% CO_2-contained incubator under 95% saturation humidity. When cells reached 60–80% confluency, transfection was performed using a lentivirus harboring the SOST sequence or the short hairpin (sh)-SOST sequence. Quantitative reverse transcription-polymerase chain reaction (qRT-PCR) and Western blot analyses were used to detect the efficiency of SOST overexpression or suppression. Stable cell lines were used for further analyses.

qRT-PCR

Total RNA was extracted from cells using TRIzol reagent (15596026, Invitrogen, Car, USA). The cDNA was synthesized with 2 mg RNA using the HiScript III RT SuperMix for qPCR (+gDNA wiper) (R323-01, Vazyme, Nanjing, China) according to the manufacturer's instructions. qRT-PCR was performed using the ABI 7500 instrument (ABI7500, ABI, USA) with SYBR Green Mix (4913914001, Roche) in a 20 μL volume reaction system containing 9 μL SYBR Mix, 0.5 μL of each primer (10 μM), 2 μL cDNA template, and 8 μL RNase free H_2O. The relative expression levels of the target genes were normalized to glyceraldehyde 3-phosphate dehydrogenase (GAPDH) and calculated using the $2^{-\Delta\Delta Ct}$ method. Primerswere synthesized by the GENERAL BIOL company (GENERAL BIOL Co., Ltd, Anhui, China). The primer sequences were shown in *Table 1*.

Western blot analysis

Total protein was extracted from the serum or heart tissues using RIPA lysis buffer (P0013, Beyotime, Shanghai, China) according to the manufacturer's instructions. The protein concentration was determined using the BCA Protein Assay Kit (70-PQ0012, MultiSciences, China) and 20 mg protein for each sample was boiled at 100 ℃ for 5 minutes. Proteins were separated using 10–12% sodium dodecyl sulfate–polyacrylamide gel electrophoresis (SDS-PAGE) and transferred onto polyvinylidene fluoride (PVDF) membranes. The membranes were then blocked with 5% lipid-free milk/Tris-buffered saline Tween (TBST) buffer for 2 hours at room temperature, followed by incubation with the following primary rabbit antibodies at 37 ℃ for 2 hours: anti-SOST (ab264040, 1:1,000, Abcam, Cambridge, UK), anti-Wnt1 (ab15251, 1:500, Abcam, Cambridge, UK), anti-β-catenin (ab32572, 1:1,000, Abcam, Cambridge, UK), anti-APC (ab40778, 1:1,000, Abcam, Cambridge, UK), and anti-GSK3β (ab32391, 1:1,000, Abcam, Cambridge, UK). Membranes were then incubated with a secondary anti-mouse IgG antibody (ab205719, 1:20,000, Abcam, Cambridge, UK) for 1–2 hours, washed with TBST and then detected immuno-complexes with ECL. Protein bands were analyzed using the Image-Pro Plus 6.0 software.

Cell proliferation and cell cycle assays

The cell proliferation ability of CFs was assessed using

the cell counting kit 8 (CCK-8; KGA317, KeyGEN Biotech, Nanjing, China), according to the manufacturer's instructions. Briefly, CFs from different groups after transfection for 48 hours were digested and seeded in 96-well plates. Cells were incubated with a culture medium containing 10 μL CCK-8 solution for 2 hours at 37 ℃. The absorbance was detected at 450 nm using a microplate reader. Cell cycles were assessed using flow cytometry (20). Briefly, CFs were harvested and fixed with 70% ethanol at 4 ℃ overnight. After staining with propidium iodide (PI, KeyGEN Biotech, Nanjing, China) for 30 minutes, flow cytometry (FACSCalibur, Becton) was performed at 488 nm. Flow cytometry results were analyzed by ModFit LT software.

Transwell invasion assays

CFs were cultured for 16 hours in serum-free medium and then resuspended. The transwell chamber was pre-coated with Matrigel (BD Biosciences) for 30 minutes at 37 ℃. Cell suspensions were transferred to the lower chambers of the transwell plates. The cells that did not invade the surface of the Matrigel membrane after incubation for 24 hours at 37 ℃ were fixed with 100% methanol and stained with 1% toluidine blue. The invasive stained cells were observed and counted using Zeiss710 light microscope (Germany).

Tube formation assay

The growth factor reduced Matrigel (BD Biosciences) was thawed in an ice bath and then rapidly added to precooled 24-well plates. After polymerization at 37 ℃ for 30 min, CMECs were suspended in 0.2% endothelial growth basal medium (EBM) and placed on the Matrigel-coated at a density of 5×10^4 cells per well. To assess the role of SOST in CMECs, conditioned medium from CMECs with suppressed or enhanced SOST expression was incubated with the CMECs for 12 h at 37 ℃ before the initiation of tube formation. CMECs were identified by morphological characteristics, and uniform "cobblestone" shape could be observed. Tube formation was defined as a structure exhibiting a length four times its width (21). Images of each group were obtained by Zeiss710 light microscope (Germany), and tube lengths were quantified using image J software (National Institutes of Health).

The myocardial infarct model

Wild-type male C57BL/6J mice, aged 8 weeks and weighing approximately 30 g, were purchased from Experimental Animal Center of Guangdong Province (Guangzhou, China). Mice were raised in a specific pathogen-free (SPF) environment under a 12-hour light/dark cycle, at 21±2 ℃ and 50–80% humidity. Animal were given free access to food and water.

Mice were randomly divided into 3 groups with 6 mice in each group. The MI model was constructed by permanent ligation of the left anterior descending coronary artery. Mice were randomly included in the study after successful modeling (22). Mice in the control group were not subjected to ligation. Histopathological changes were assessed to determine the extent of cardiac remodeling at 28 days after MI. Lentivirus harboring the SOST sequence or the sh-SOST sequence was injected into the tail vein of mice at 24 hours after MI. qRT-PCR and Western blot analyses were used to confirm SOST overexpression or suppression. Animal experiments were performed under a project license (ZF2019-405-01) granted by the Ethics Committee of Guangdong Provincial Hospital of Chinese Medicine, in compliance with the NIH Guide for the Care and Use of Laboratory Animals, 8th edition.

Echocardiographic measurement

Prior to sacrificing the animals, the echocardiographic LV function of the mice was assessed using a Vevo 770 echocardiography system (Visual Sonics, Toronto, Canada) equipped with a 15L8 linear array transducer. Mice were anesthetized with 1.5% isoflurane mixed with oxygen and placed in the supine position on a heating pad. After removal of hair, pre-warmed ultrasound transmission gel (Aquasonic, Parker Laboratory, Fairfield, NJ, USA) was applied to the precordial region.

Short axis measurements were used to capture M-mode tracing at the level of the papillary muscles with 25 mm signal depth. Values were averaged over three to six consecutive cardiac cycles.

Enzyme linked immunosorbent assay (ELISA)

Human and mice serum levels of SOST were detected by human SOST ELISA kit (Abcam, ab155440) and mouse SOST ELISA kit (Abcam, ab213889), respectively. Assays

were performed following the manufacturer's instructions.

Histopathological changes analysis

Hematoxylin and eosin (H&E), Masson staining, and Sirius red staining (KeyGEN Biotech, Nanjing, China) were used to stain mice myocardial tissues. Heart tissues were sliced into 8 μm-thick sections and fixed with 4% paraformaldehyde at room temperature. After staining, the sections were dehydrated, sealed with neutral gum, then subsequently rinsed with running water and visualized under an Olympus light microscope (Japan).

Immunohistochemical staining

Immunohistochemistry was used to detect the expression of proteins involved in the Wnt signaling pathway, including Wnt1, β-catenin, adenomatous polyposis coli (APC), and glycogen synthase kinase (GSK) 3β. Briefly, samples were fixed in 10% formaldehyde and embedded in paraffin. Serial slides (4 μm thick) were generated and placed in 3% catalase for 15 minutes, followed by blocking with 50 μL goat serum for 20 minutes at room temperature. Subsequently, sections were incubated with the following primary rabbit antibodies: anti-SOST (ab264040, 1:1,000, Abcam, Cambridge, UK), anti-Wnt1 (ab15251, 1:500, Abcam, Cambridge, UK), anti-β-catenin (ab32572, 1:1,000, Abcam, Cambridge, UK), anti-APC (ab40778, 1:1,000, Abcam, Cambridge, UK), or anti-GSK3β (ab32391, 1:1,000, Abcam, Cambridge, UK) at 37 ℃ for 2 hours. The sections were then washed 3 times with phosphate buffered saline (PBS) and incubated with a FITC-conjugated goat anti-rabbit IgG (ab6785, Abcam, Cambridge, UK, 1:1,000) at 37 ℃ for 1 hour after. A DAPI dye solution (50–100 mL) was added to each section and placed in the dark at room temperature for 5 minutes. Sections were then sealed with an anti-extractant sealant and visualized with the XSP-36 microscope (Boshida Optical Co., Ltd, Shenzhen, China).

Statistical analysis

Data are presented as mean ± standard deviation (SD) from at least 3 independent experiments performed in triplicate. Unpaired t tests and one-way analysis of variance (ANOVA) were used to perform statistical comparisons between two groups and more than two groups, respectively. All statistical analyses were completed with the SPSS 22.0 software (IBM, Armonk, NY, USA) and a P value <0.05 was considered statistically significant.

Results

SOST was significantly elevated in patients with cardiac remodeling after MI

According to the inclusion and exclusion criteria, a total of 54 patients with MI were enrolled, including 29 patients with LV remodeling and 25 patients without remodeling. A total of 12 healthy subjects were included in the control group. Consistent with our previous results (17), the expression of SOST was significantly increased in patients with post-MI cardiac remodeling compared to patients without cardiac remodeling (*Figure 1A*). This was confirmed by Western blot analysis at the protein level (*Figure 1B*). ELISA assays further verified that the levels of SOST were significantly elevated in the cardiac remodeling group (*Figure 1C*). These results demonstrated that serum SOST was significantly elevated in patients with cardiac remodeling after MI, suggesting that SOST might play a crucial role in the process of cardiac remodeling.

SOST inhibited angiogenesis of CMECs and increased the proliferation and migration of CFs

A study has shown that the angiogenesis of CMECs and the proliferation of CFs participate in the development of cardiac remodeling (23). To investigate the effects of SOST in angiogenesis, CMECs were transfected with lentivirus to generate CMECs that overexpressed SOST and CMECs in which SOST expression was suppressed. The transfection efficiency was confirmed by qRT-PCR and Western blot analyses (*Figure 2A*,*2B*). As shown in *Figure 2C*, the number of capillary-like structures was significantly decreased in cells overexpressing SOST, and significantly increased in cells transfected with sh-SOST compared with negative control cells. Further analysis showed that the tube length of CMECs overexpressing SOST was shorter than that in the control group, while CMECs transfected with sh-SOST had longer tube length compared to the control group (*Figure 2C*). These results indicated that SOST could reduce the angiogenesis of CMECs.

In addition, CCK-8 assays demonstrated that CFs overexpressing SOST showed dramatically increased the cell viability, while suppressing SOST significantly decreased cell viability in CFs compared with control cells at 48 and 72 hours (*Figure 2D*). Cell cycle analysis showed

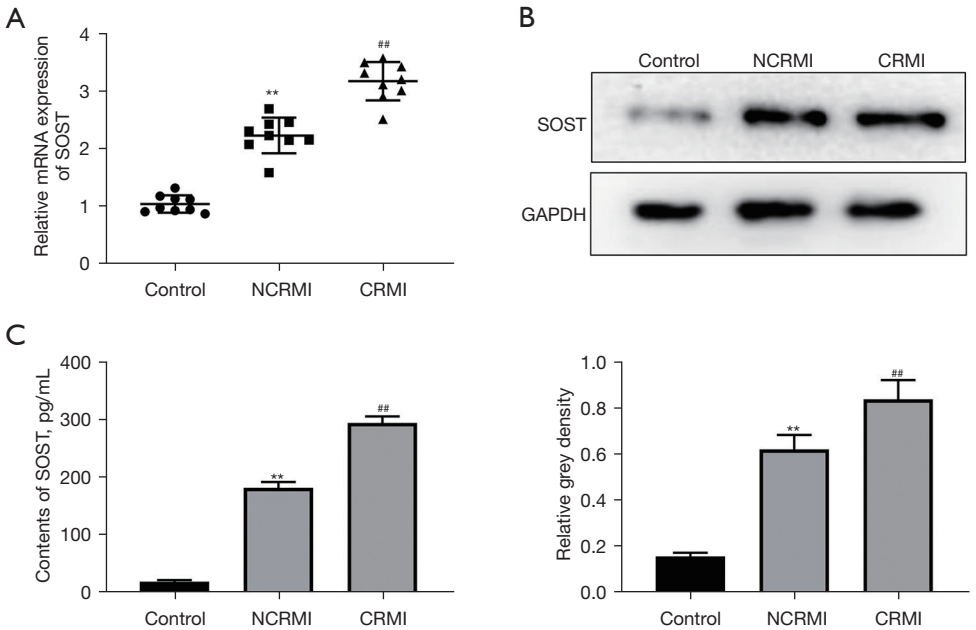

Figure 1 SOST was significantly elevated in patients with cardiac remodeling after MI. (A) The mRNA expression of SOST in the serum of patients with post-MI cardiac remodeling was detected by qRT-PCR. (B) Western blot analysis was performed to assess the protein expression of SOST, with GAPDH as an internal control. (C) ELISA was conducted to detect the expression of SOST. The data are presented as mean ± SD. **P<0.01, NCRMI group *vs*. control group; ##P<0.01, CRMI group *vs*. NCRMI group. MI, myocardial infarction; SOST, sclerostin; CRMI, cardiac remodeling after MI; NCRMI, no cardiac remodeling after MI; GAPDH, glyceraldehyde 3-phosphate dehydrogenase; qRT-PCR, quantitative real-time polymerase chain reaction; ELISA, enzyme-linked immunosorbent assay; SD, standard deviation.

that the proportion of CFs staged in the G1 period was increased in cells overexpressing SOST, while the proportion of cells in the S and G2 cycles was significantly decreased compared with the control group. However, the converse was observed in cells transfected with sh-SOST compared with control cells (*Figure 2E*). In addition, the migration ability of CFs was dramatically elevated in the SOST-overexpression group, and significantly reduced in the SOST-silenced group compared with control cells (*Figure 2F*). These findings suggested that SOST could promote the proliferation and migration of CFs.

The expression of Wnt signaling marker proteins was affected by SOST

SOST can participate in various pathophysiological processes associated with the Wnt signaling pathway (8,24). To evaluate whether the increased proliferation of CFs induced by SOST is related to the Wnt signaling pathway, the protein markers including Wnt1, β-catenin, APC, and GSK3β were assessed by qRT-PCR and Western blot analysis. As shown in *Figure 3A*, the mRNA expression of Wnt1 and β-catenin were significantly downregulated in the SOST-overexpression group, and upregulated in the SOST-silenced group, compared with the control group. However, the expression of APC and GSK3β showed the opposite results. These data were confirmed by Western blot analysis (*Figure 3B*). Moreover, similar trends were observed with CMECs (data not shown). These results indicated that SOST inhibited the angiogenesis of CMECs and promoted the cell development of CFs via Wnt signaling pathway.

SOST was significantly elevated in mice with post-infarction cardiac remodeling

To further investigate the function of SOST in post-infarction cardiac remodeling, a mouse model with MI was established. Echocardiographic measurements showed that the left ventricular end diastolic dimension (LVEDD) and the left ventricular end systolic dimension (LVESD)

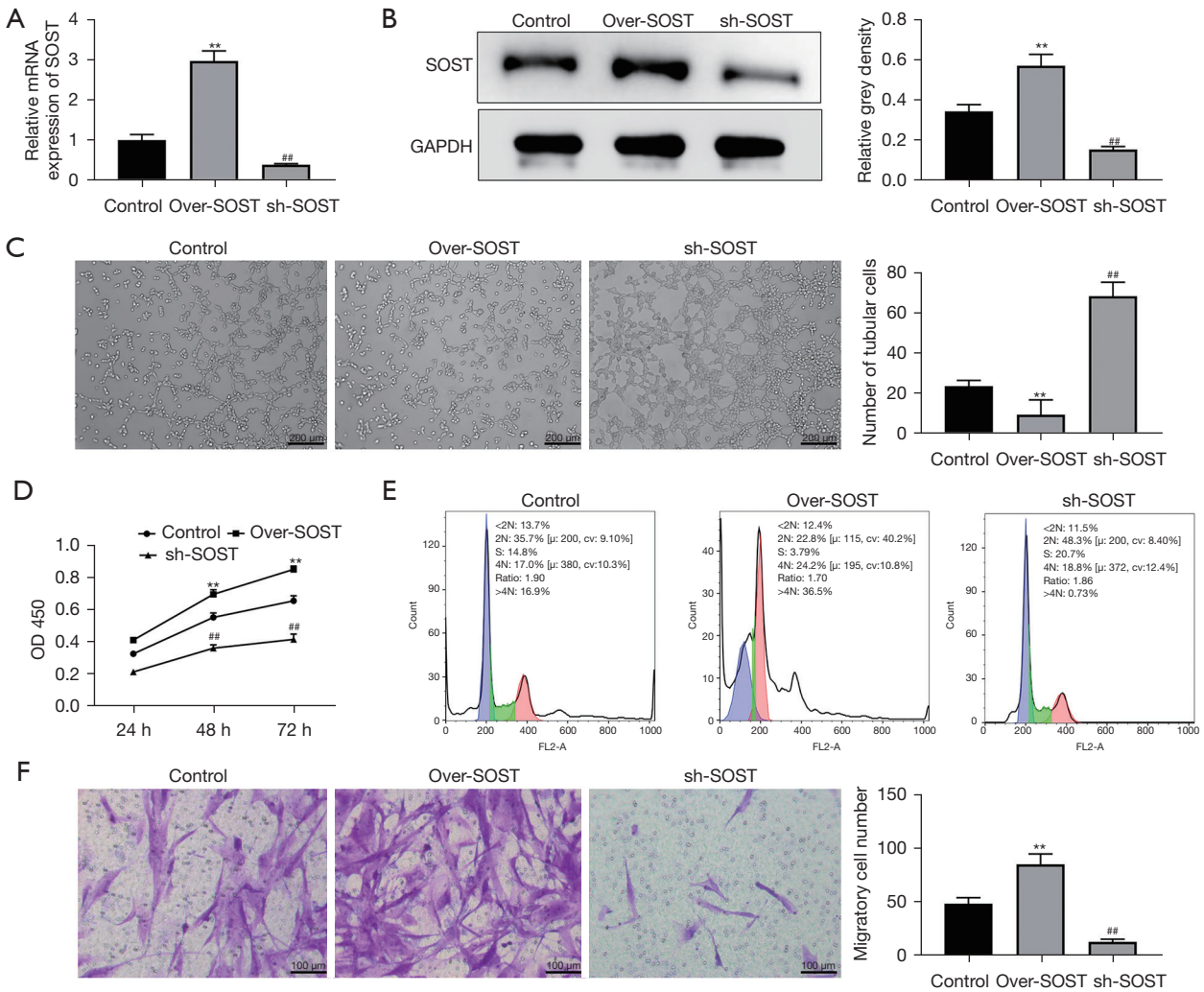

Figure 2 SOST inhibited angiogenesis of CMECs and promoted the proliferation and migration of CFs. (A) The mRNA expression of SOST in cells transfected with the SOST overexpression vector and cells transfected with the sh-SOST vector was detected using qRT-PCR. GAPDH was used as the normalization control. (B) The protein expression of SOST in cells transfected with the SOST overexpression vector and cells transfected with the sh-SOST vector was detected with Western blot. GAPDH was used as the normalization control. (C) The tube formation and number of capillary-like structures in cells overexpressing SOST and cells transfected with the sh-SOST vector. (D) CCK-8 assay to detect the cell viability of CFs when overexpressing or suppressing SOST at 24, 48 and 72 h, respectively. (E) The cell cycle of CFs was detected by flow cytometry in cells overexpressing SOST and cells with suppressed SOST expression. (F) CFs were stained with propidium iodide. The migration ability of CFs was detected using the Transwell assay. The data are presented as mean ± SD. **P<0.01, SOST-overexpression group *vs.* control group; ##P<0.01, sh-SOST group *vs.* control group. SOST, sclerostin; sh, short hairpin; CMEC, cardiac microvascular endothelial cell; CF, cardiac fibroblast; qRT-PCR, quantitative real-time polymerase chain reaction; GAPDH, glyceraldehyde 3-phosphate dehydrogenase; CCK-8, cell counting kit 8; SD, standard deviation.

were dramatically increased in the model group (*Figure 4A*, Table S1). H&E, Masson, and Sirius Red staining revealed increased myocardial inflammatory infiltration, increased myocyte cross-sectional area, and fibrotic areas in mice with cardiac remodeling compared with the sham group (*Figure 4A*), indicating that the model was successfully established. Further analysis showed that expression of SOST was significantly increased in the cardiac remodeling group compared to the sham group both at the mRNA and protein level (*Figure 4B*,*4C*). ELISA analysis also showed

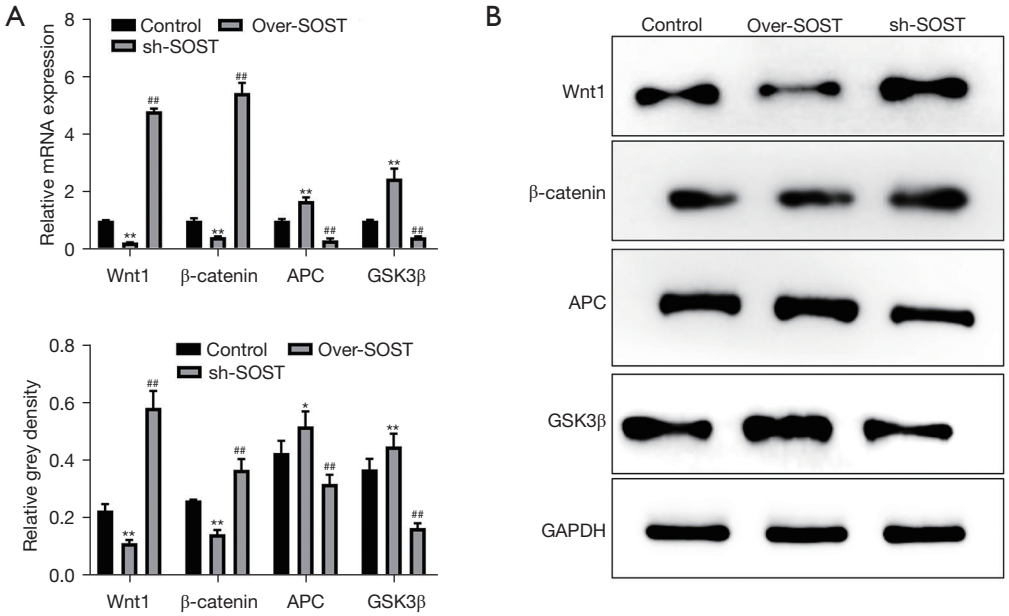

Figure 3 The expression of the Wnt pathway marker proteins was affected by SOST. (A) The mRNA expression of the Wnt pathway marker genes, including Wnt1, β-catenin, APC, and GSK3β, was detected by qRT-PCR. (B) Western blot was used to detect the protein expression of Wnt1, β-catenin, APC, and GSK3β. GAPDH was used as the internal control. The data are presented as the mean ± SD (n=3). *P<0.05, SOST-overexpression group *vs.* control group; **P<0.01, SOST-overexpression group *vs.* control group; ##P<0.01, sh-SOST group *vs.* control group. SOST, sclerostin; sh, short hairpin; APC, adenomatous polyposis coli; GSK3β, glycogen synthase kinase 3β; qRT-PCR, quantitative real-time polymerase chain reaction; GAPDH, glyceraldehyde 3-phosphate dehydrogenase; SD, standard deviation.

that the content of SOST in the cardiac remodeling group was dramatically elevated compared to the model group and the sham group (*Figure 4D*).

SOST exacerbated postinfarct pathological myocardial remodeling in vivo

To further confirm the function of SOST in cardiac remodeling after MI, loss and gain of function for SOST was performed. qRT-PCR and Western blot analysis showed that the expression of SOST was significantly overexpressed or suppressed in the SOST-overexpression group and the sh-SOST group, respectively (*Figure 5A,5B*). Echocardiographic measurements showed that overexpression of SOST increased LVEDD and LVESD, and suppression of SOST decreased LVEDD and LVESD compared to the model group (*Figure 5C*, Table S1). The significant increase in LV chamber diameter was accompanied by a decline in LV function with decreases in both ejection fraction (EF) and fractional shortening (FS) (*Figure 5C*, Table S1).

H&E, Masson, and Sirius Red staining revealed that overexpression of SOST greatly aggravated inflammatory infiltration, myocyte cross-sectional area, and fibrosis of the heart, while inflammatory infiltration and fibrosis were dramatically reduced when SOST was suppressed (*Figure 5D*). Moreover, overexpressing SOST resulted in reduced capillary density compared to the control group (*Figure 5D*). Capillary density was increased in the SOST-suppressed group compared with vehicle-treated mice (*Figure 5D*). The LV dilation and dysfunction in the infarcted hearts of the SOST-overexpression group indicate the occurrence and progression of heart failure, demonstrating that SOST plays a key role in post-MI cardiac remodeling.

Wnt signaling marker proteins were affected by SOST in vivo

To confirm whether SOST could affect the Wnt signaling pathway, qRT-PCR and Western blot were used to detect the Wnt signaling-related protein markers. The results showed that the expression of APC and GSK3β were significantly elevated in the SOST-overexpression group, and markedly decreased in the sh-SOST group, compared

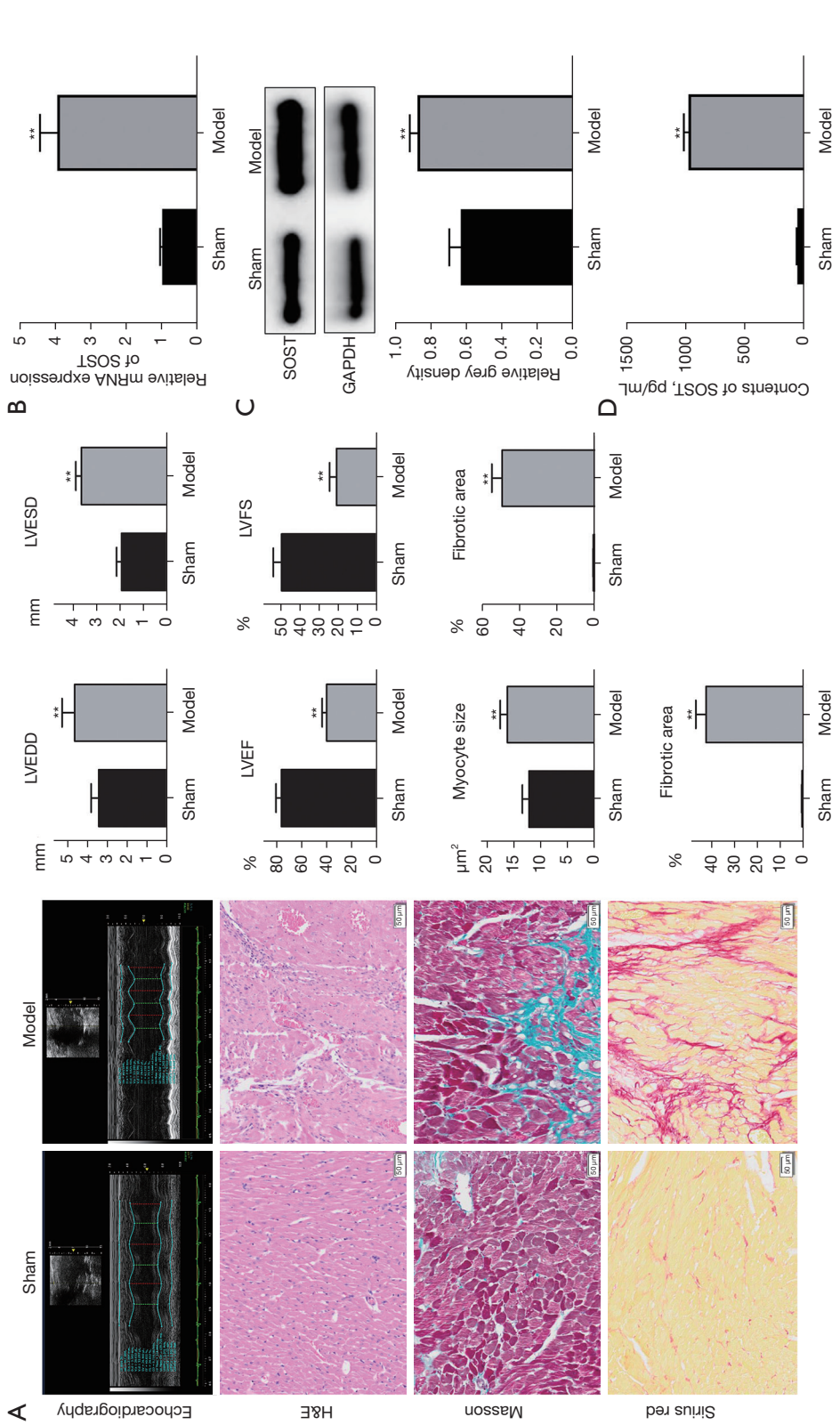

Figure 4 SOST was significantly elevated in the *in vivo* MI model. (A) Echocardiographic measurements and histochemical staining analyses, including H&E, Masson, and Sirius Red staining, were performed to confirm the successful construction of the MI model (Bar =50 μm). Quantitative analysis of LVEDD, LVESD, LVEF, LVFS, myocyte size and fibrotic area are shown in the right panels. (B) The mRNA expression of SOST in the heart tissues was detected by qRT-PCR. (C) Western blot was used to detect the protein expression of SOST in the heart tissues, with GAPDH as the internal control. (D) ELISA was performed to detect the contents of SOST in the different groups. The data are presented as the mean ± SD (n=3). **P<0.01, model group *vs.* sham group. SOST, sclerostin; H&E, hematoxylin and eosin; LVEDD, left ventricular end diastolic dimension; LVESD, left ventricular end systolic dimension; LVEF, left ventricular ejection fraction; LVFS, left ventricular fractional shortening; MI, myocardial infarction; GAPDH, glyceraldehyde 3-phosphate dehydrogenase; SD, standard deviation.

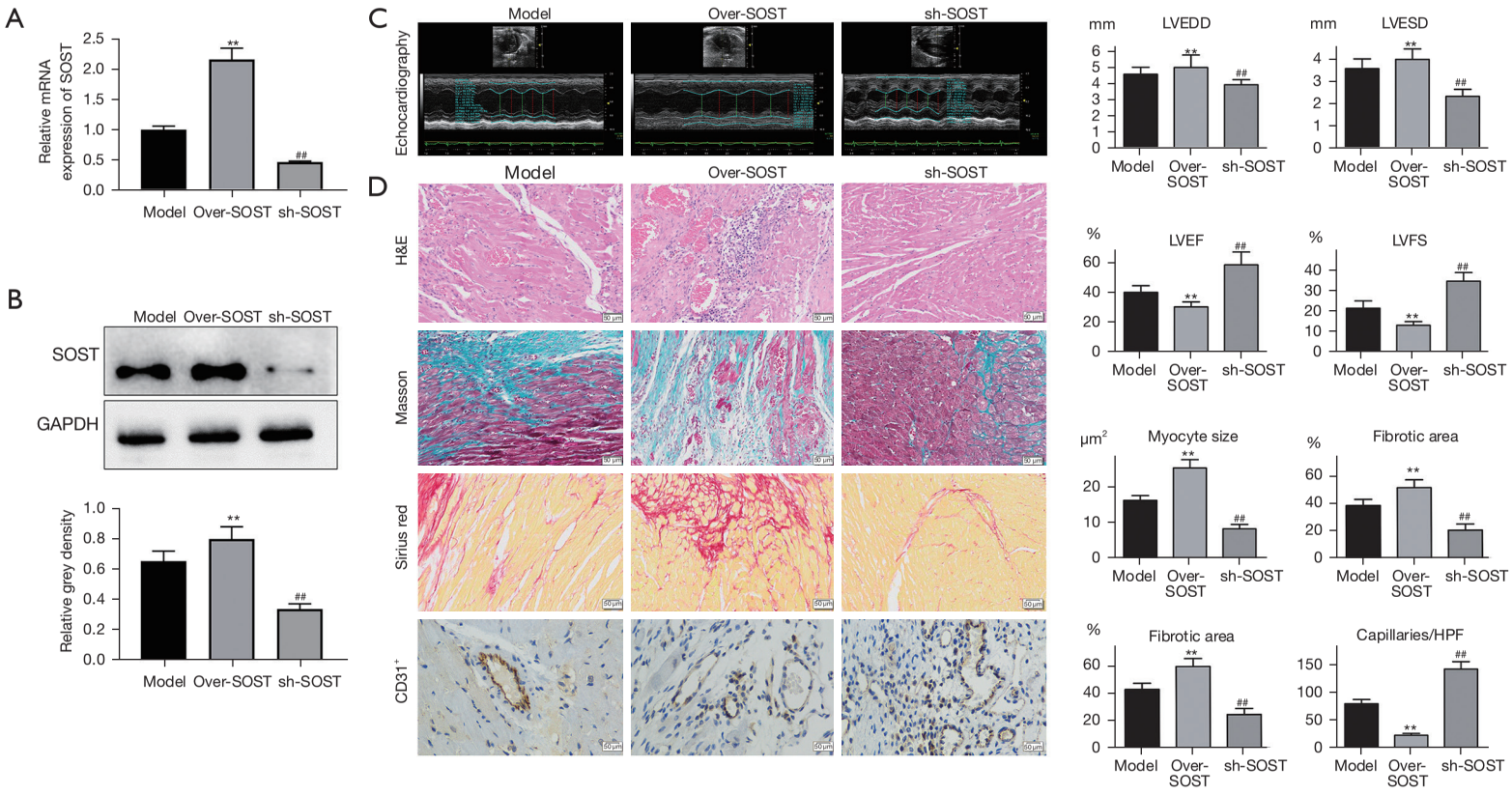

Figure 5 SOST exacerbated the postinfarct pathological myocardial remodeling *in vivo*. (A,B) qRT-PCR and Western blot analysis to detect the expression of SOST in the SOST-overexpression group and the sh-SOST group, respectively. GAPDH was used as the internal control. (C,D) Echocardiographic measurements and histochemical staining analyses, including H&E, Masson, Sirius Red staining and $CD31^+$ capillaries, to assess the effects of SOST on cardiac remodeling after MI *in vivo* (Bar =50 μm). Quantitative analysis of LVEDD, LVESD, LVEF, LVFS, myocyte size, fibrotic area, and $CD31^+$ capillaries are shown in the right panel. The data are presented as mean ± SD. **P<0.01, SOST-overexpression group *vs.* model group; ##P<0.01, sh-SOST group *vs.* model group. SOST, sclerostin; sh, short hairpin; GAPDH, glyceraldehyde 3-phosphate dehydrogenase; H&E, hematoxylin and eosin; LVEDD, left ventricular end diastolic dimension; LVESD, left ventricular end systolic dimension; LVEF, left ventricular ejection fraction; LVFS, left ventricular fractional shortening; qRT-PCR, quantitative real-time polymerase chain reaction; SD, standard deviation.

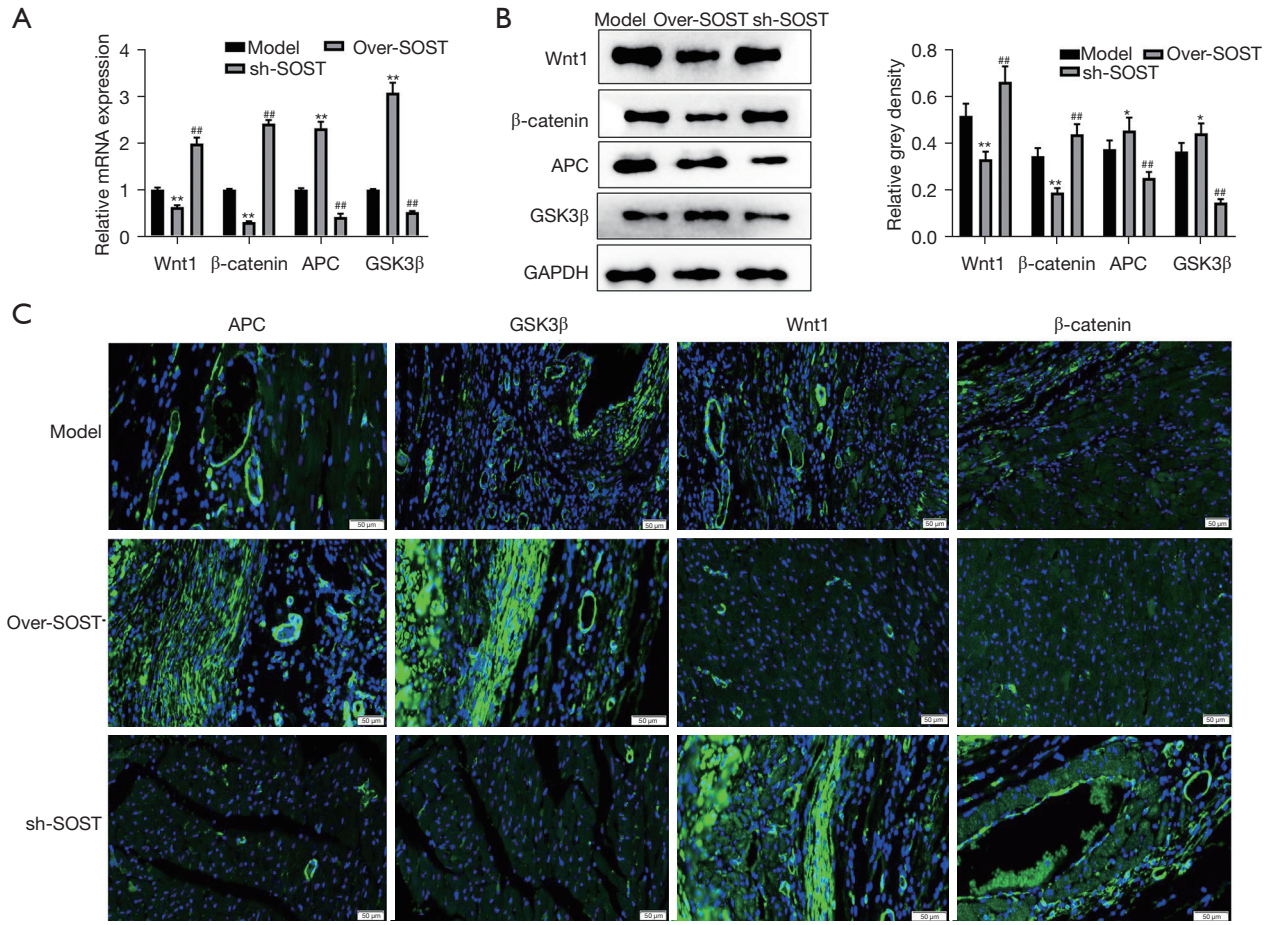

Figure 6 The expression of Wnt signaling marker proteins was affected by SOST *in vivo*. (A) The expression of Wnt signaling marker genes was detected by qRT-PCR, including Wnt1, β-catenin, APC, and GSK3β. (B) Western blot was used to detect the protein expression of Wnt1, β-catenin, APC, and GSK3β. GAPDH was used as the internal control. (C) Immunofluorescence assays were performed to detect the expression of the Wnt signaling marker proteins (Bar =50 μm). Immunohistochemical staining: green fluorescence marks the corresponding protein and blue fluorescence marks the nucleus. The data are presented as the mean ± SD. *P<0.05, SOST-overexpression group *vs.* model group; **P<0.01, SOST-overexpression group *vs.* model group; ##P<0.01, sh-SOST group *vs.* model group. SOST, sclerostin; sh, short hairpin; APC, adenomatous polyposis coli; GSK3β, glycogen synthase kinase 3β; GAPDH, glyceraldehyde 3-phosphate dehydrogenase; qRT-PCR, quantitative real-time polymerase chain reaction; SD, standard deviation.

with the control group both at the mRNA and protein levels (*Figure 6A*,*6B*). Immunofluorescence analysis showed that the fluorescence signal of APC and GSK3β was significantly enhanced in the SOST-overexpression group and markedly decreased in the sh-SOST group compared with the control group (*Figure 6C*). Conversely, the expression of Wnt 1 and B-catenin were markedly reduced in the SOST-overexpression group, but enhanced in the sh-SOST group compared to the control group. These results suggested that SOST exacerbated post-infarction cardiac remodeling, and this was associated with the Wnt signaling pathway.

Discussion

MI is characterized by the rapid death of large numbers of cardiomyocytes, triggering a series of molecular and cellular remodeling, including inflammatory response, microcirculatory dysfunction, cardiomyocyte hypertrophy, fibrosis, and collagen scar formation. Cardiac remodeling is the primary mechanism of heart failure and sudden death. In the early stage, reconstruction can maintain the integrity and function of the heart, but continuous reconstruction eventually leads to LV dilation and

cardiac insufficiency, followed by progression to heart failure (25). Therefore, delaying or even improving the pathophysiological remodeling process after MI may be an important therapeutic intervention after cardiac injury. The present study demonstrated that SOST deteriorated cardiac dysfunction and dilatation, decreased angiogenesis of CMECs and capillary density, increased the proliferation of CFs and LV fibrosis, and attenuated Wnt/β-catenin signaling. These data indicated that inhibiting the function of SOST may have therapeutic potential in the myocardial remodeling response to infarction.

A variety of pathophysiological factors affect the process of myocardial remodeling after infarction. However, the infarct size and the degree of repair after infarction are the decisive factors that determine this process and the occurrence of heart failure (25). Increasing evidence has shown that inflammation plays an important role in myocardial remodeling after MI, and this is characterized by significant infiltration of inflammatory cells, cytokines, and chemokines to the infarct area (26,27). In a previous study, several novel biomarkers of cardiac remodeling were identified using cytokine antibody arrays, including SOST, growth differentiation factor-15, urokinase-type plasminogen activator, midkine, and monocyte chemotactic protein-3. Out of these biomarkers, SOST showed the most significant elevation following myocardial remodeling (17). Consistent with previous studies, the present data confirmed that SOST was significantly increased during cardiac remodeling, both *in vivo* and *in vitro*, suggesting that SOST plays an essential role in cardiac remodeling. In fact, SOST has been demonstrated to participate in various cardiovascular diseases, and circulating levels of SOST are considered to be associated with cardiovascular mortality (12-14). Recently, it was shown that SOST genetic variants were associated with a higher risk of MI. However, the detailed mechanisms of SOST in cardiac remodeling remain to be fully elucidated.

The pathophysiological mechanisms responsible for cardiac remodeling include cardiomyocyte hypertrophy, microvascular rarefaction, and extracellular matrix remodeling (28). Cardiomyocyte hypertrophy and apoptosis, as well as excessive increases in the number of CFs contribute to the long-term oxidation response during cardiac remodeling (29). Fibroblasts are enmeshed within the interstitial and perivascular extracellular matrix (30). It has been demonstrated that cardiac myofibroblasts not only respond to proinflammatory cytokines, but also promote the secretion of various bioactive molecules including cytokines, vasoactive peptides, and growth factors under mechanical stretch and changes in oxygen availability in cardiac remodeling (28,31). Furthermore, the targeted ablation of periostin-expressing activated fibroblasts prevents adverse cardiac remodeling in mice (32). In addition, non-oxidizable high mobility group box protein 1 (HMGB1)-induced CF migration occurs via C-X-C chemokine receptor type 4 (CXCR4) in a C-X-C motif chemokine ligand 12 (CXCL12)-independent manner and is exacerbated during tissue remodeling after MI (33). Consistent with these findings, we found that overexpression of SOST promote the proliferation of CFs, whereas downregulation of SOST inhibited the process. These results demonstrated that SOST-mediated cardiac remodeling is related to the enhanced proliferation of CFs.

CMECs are the major cell type in the heart, and the vascular microenvironment is crucial in maintaining normal cardiac function and pathological remodeling. Dysregulated response of the CMECs in atherosclerotic plaques may promote plaque rupture, leading to MI (34). Brahma-related gene1/Brahma-associated factor 60a (BAF60a) deficiency in CMECs prevented abdominal aortic aneurysm by reducing inflammation and extracellular matrix degradation, suggesting that CMECs might participate in MI by regulating inflammation (35). SOST is considered to be a regulatory molecule in vascular media calcification and in the bone-vascular axis, and thus, may play a critical role in CMECs (36). Indeed, it has been demonstrated that SOST is expressed in CMECs of atherosclerotic plaques, suggesting a potential role for this protein in the development of atherosclerosis, which may lead to MI (11). The present investigation showed that overexpression of SOST inhibited the angiogenesis of CMECs and capillary density in mice heart after MI, while suppression of SOST promoted the angiogenesis of CMECs and capillary density in the myocardium. These results demonstrated that SOST-induced angiogenesis inhibition may aggravate adverse cardiac remodeling.

SOST is a well-known inhibitor of bone formation that acts on the Wnt/β-catenin signaling pathway. SOST has been shown to participate in different processes with pleiotropic cellular function, including cell development of retinoblastoma cells and CFs, cell growth, energy metabolism and extracellular matrix remodeling (37,38). Increasingly, studies have demonstrated that Wnt signaling plays a crucial role in cardiovascular diseases related to

vascular calcification, by inducing different physiological and pathological effects on cardiovascular functions (39,40). Angiogenesis is a key process in the restoration of blood supply to the infarct area after MI. Wnt1, a ligand of Wnt/β-catenin signaling, promotes pro-angiogenesis and reduces the infarct size (41). *In vitro* studies have implicated the Wnt1/β-catenin pathway as a promoter of endothelial cell proliferation (42,43). *In vivo*, increased HO-1 expression and Wnt1/β-catenin signaling pathway can reduce infarct size and attenuate cardiac remodeling in MI mice (44). In addition, GSK-3β inhibitors increased the expression of β-catenin in endothelial cells, limiting cardiac remodeling and promoting angiogenesis (45). These data suggest that Wnt/β-catenin overexpression is able to reduce infarct size and to improve cardiac function by decreasing apoptosis and increasing angiogenesis. There are also many studies that Wnt signaling pathway significantly participates in cardiac fibrosis pathogenesis (46,47). Recently, it was demonstrated that the SOST/receptor-related protein 4 and ginkgo biloba extract alleviated β-glycerophosphate-induced vascular smooth muscle cell calcification by inhibiting the Wnt/β-catenin pathway (48). These results suggested that CMEC development may be regulated by the Wnt/β-catenin pathway. However, to date, there have been no reports examining the mechanisms of SOST, mediated by the Wnt signaling pathway, in CMECs during cardiac remodeling. The present study demonstrated that overexpression of SOST blocked the activation of the Wnt signaling pathway both *in vivo* and *in vitro*, demonstrating that SOST affected CMECs by regulating Wnt signaling pathway during cardiac remodeling.

Conclusions

In summary, this study presented novel findings demonstrating that SOST aggravates cardiac remodeling and dysfunction after MI, and this is associated with the Wnt signaling pathway. Indeed, SOST may be a novel biomarker and potential therapeutic target for detrimental cardiac remodeling.

Acknowledgments

The authors gratefully acknowledge the contributions of all the investigators of the program.
Funding: This study was funded by the National Science Foundation (grant No. 81703877), the Science and Technology Planning Project of Guangzhou (202102010301), the Featured Innovative Project from Guangdong Provincial Universities (2019KTSCX029), the Young Talents Support Project from China Association of Chinese Medicine (2019-QNRC2-C06), the Team of Prevention and Treatment of Acute Myocardial Infarction with Chinese Medicine (2019KCXTD009), and the Foundation of Guangdong Province of Chinese Medicine (20211187&20201142). The sponsors have had no role in the project development, the collection of data, the preparation of the manuscript, nor the decision to publish.

Footnote

Reporting Checklist: The authors have completed the ARRIVE reporting checklist (available at https://jtd.amegroups.com/article/view/10.21037/jtd-22-473/rc).

Data Sharing Statement: Available at https://jtd.amegroups.com/article/view/10.21037/jtd-22-473/dss

Conflicts of Interest: All authors have completed the ICMJE uniform disclosure form (available at https://jtd.amegroups.com/article/view/10.21037/jtd-22-473/coif). The authors have no conflicts of interest to declare.

Ethical Statement: The authors are accountable for all aspects of the work in ensuring that questions related to the accuracy or integrity of any part of the work are appropriately investigated and resolved. All participants signed the project informed consent forms. The Ethics Committee of Guangdong Provincial Hospital of Chinese Medicine approved this project (Z2017-080-01). The study was conducted in accordance with the Declaration of Helsinki (as revised in 2013). Animal experiments were performed under a project license (ZF2019-405-01) granted by the Ethics Committee of Guangdong Provincial Hospital of Chinese Medicine, in compliance with the NIH Guide for the Care and Use of Laboratory Animals, 8th edition.

References

1. Dai J, Su Y, Zhong S, et al. Exosomes: key players in cancer and potential therapeutic strategy. Signal Transduct Target Ther 2020;5:145.
2. Wu X, Reboll MR, Korf-Klingebiel M, et al. Angiogenesis after acute myocardial infarction. Cardiovasc Res 2021;117:1257-73.
3. Raziyeva K, Smagulova A, Kim Y, et al. Preconditioned and Genetically Modified Stem Cells for Myocardial Infarction Treatment. Int J Mol Sci 2020;21:7301.
4. Song J, Kim YK. Discovery and Functional Prediction of Long Non-Coding RNAs Common to Ischemic Stroke and Myocardial Infarction. J Lipid Atheroscler 2020;9:449-59.
5. Veeraveedu PT, Sanada S, Okuda K, et al. Ablation of IL-33 gene exacerbate myocardial remodeling in mice with heart failure induced by mechanical stress. Biochem Pharmacol 2017;138:73-80.
6. Yang M, Liu X, Jiang M, et al. miR-543 in human mesenchymal stem cell-derived exosomes promotes cardiac microvascular endothelial cell angiogenesis after myocardial infarction through COL4A1. IUBMB Life 2021;73:927-40.
7. Pepin ME, Drakos S, Ha CM, et al. DNA methylation reprograms cardiac metabolic gene expression in end-stage human heart failure. Am J Physiol Heart Circ Physiol 2019;317:H674-84.
8. Weivoda MM, Youssef SJ, Oursler MJ. Sclerostin expression and functions beyond the osteocyte. Bone 2017;96:45-50.
9. Ma J, Zhang X, Zhang H, et al. lncRNA MEG3 Suppresses the Progression of Ankylosis Spondylitis by Regulating the Let-7i/SOST Axis. Front Mol Biosci 2020;7:173.
10. Zwakenberg SR, van der Schouw YT, Schalkwijk CG, et al. Bone markers and cardiovascular risk in type 2 diabetes patients. Cardiovasc Diabetol 2018;17:45.
11. Leto G, D'Onofrio L, Lucantoni F, et al. Sclerostin is expressed in the atherosclerotic plaques of patients who undergoing carotid endarterectomy. Diabetes Metab Res Rev 2019;35:e3069.
12. Novo-Rodríguez C, García-Fontana B, Luna-Del Castillo JD, et al. Circulating levels of sclerostin are associated with cardiovascular mortality. PLoS One 2018;13:e0199504.
13. Zeng C, Guo C, Cai J, et al. Serum sclerostin in vascular calcification and clinical outcome in chronic kidney disease. Diab Vasc Dis Res 2018;15:99-105.
14. He W, Li C, Chen Q, et al. Serum sclerostin and adverse outcomes in elderly patients with stable coronary artery disease undergoing percutaneous coronary intervention. Aging Clin Exp Res 2020;32:2065-72.
15. Kanbay M, Solak Y, Siriopol D, et al. Sclerostin, cardiovascular disease and mortality: a systematic review and meta-analysis. Int Urol Nephrol 2016;48:2029-42.
16. Bovijn J, Krebs K, Chen CY, et al. Evaluating the cardiovascular safety of sclerostin inhibition using evidence from meta-analysis of clinical trials and human genetics. Sci Transl Med 2020;12:eaay6570.
17. Mao S, Liang Y, Chen P, et al. In-depth proteomics approach reveals novel biomarkers of cardiac remodelling after myocardial infarction: An exploratory analysis. J Cell Mol Med 2020;24:10042-51.
18. Li JH, Dai J, Han B, et al. MiR-34a regulates cell apoptosis after myocardial infarction in rats through the Wnt/β-catenin signaling pathway. Eur Rev Med Pharmacol Sci 2019;23:2555-62.
19. Liu FJ. LncRNA-P21 suppresses apoptosis of myocardial cells in rats with acute myocardial infarction via regulating Wnt/beta-catenin signaling pathway. Eur Rev Med Pharmacol Sci 2020;24:10078-85.
20. Darzynkiewicz Z, Bedner E, Smolewski P. Flow cytometry in analysis of cell cycle and apoptosis. Semin Hematol 2001;38:179-93.
21. Ma FX, Zhou B, Chen Z, et al. Oxidized low density lipoprotein impairs endothelial progenitor cells by regulation of endothelial nitric oxide synthase. J Lipid Res 2006;47:1227-37.
22. Mao S, Chen P, Li T, et al. Tongguan Capsule Mitigates Post-myocardial Infarction Remodeling by Promoting Autophagy and Inhibiting Apoptosis: Role of Sirt1. Front Physiol 2018;9:589.
23. Zhang Y, Zhu Z, Wang T, et al. TGF-β1-containing exosomes from cardiac microvascular endothelial cells mediate cardiac fibroblast activation under high glucose conditions. Biochem Cell Biol 2021;99:693-9.
24. Kim SP, Da H, Wang L, et al. Bone-derived sclerostin and Wnt/β-catenin signaling regulate PDGFRα+ adipoprogenitor cell differentiation. FASEB J 2021;35:e21957.
25. Pluijmert NJ, Bart CI, Bax WH, et al. Effects on cardiac function, remodeling and inflammation following myocardial ischemia-reperfusion injury or unreperfused myocardial infarction in hypercholesterolemic APOE*3-Leiden mice. Sci Rep 2020;10:16601.
26. Wang Y, Zhao R, Shen C, et al. Exosomal CircHIPK3 Released from Hypoxia-Induced Cardiomyocytes Regulates Cardiac Angiogenesis after Myocardial Infarction. Oxid Med Cell Longev 2020;2020:8418407.
27. Kologrivova I, Shtatolkina M, Suslova T, et al. Cells of the

Immune System in Cardiac Remodeling: Main Players in Resolution of Inflammation and Repair After Myocardial Infarction. Front Immunol 2021;12:664457.
28. Porter KE, Turner NA. Cardiac fibroblasts: at the heart of myocardial remodeling. Pharmacol Ther 2009;123:255-78.
29. Shinde AV, Frangogiannis NG. Fibroblasts in myocardial infarction: a role in inflammation and repair. J Mol Cell Cardiol 2014;70:74-82.
30. Plikus MV, Wang X, Sinha S, et al. Fibroblasts: Origins, definitions, and functions in health and disease. Cell 2021;184:3852-72.
31. Ivey MJ, Kuwabara JT, Pai JT, et al. Resident fibroblast expansion during cardiac growth and remodeling. J Mol Cell Cardiol 2018;114:161-74.
32. Kaur H, Takefuji M, Ngai CY, et al. Targeted Ablation of Periostin-Expressing Activated Fibroblasts Prevents Adverse Cardiac Remodeling in Mice. Circ Res 2016;118:1906-17.
33. Di Maggio S, Milano G, De Marchis F, et al. Non-oxidizable HMGB1 induces cardiac fibroblasts migration via CXCR4 in a CXCL12-independent manner and worsens tissue remodeling after myocardial infarction. Biochim Biophys Acta Mol Basis Dis 2017;1863:2693-704.
34. Derda AA, Woo CC, Wongsurawat T, et al. Gene expression profile analysis of aortic vascular smooth muscle cells reveals upregulation of cadherin genes in myocardial infarction patients. Physiol Genomics 2018;50:648-57.
35. Chang Z, Zhao G, Zhao Y, et al. BAF60a Deficiency in Vascular Smooth Muscle Cells Prevents Abdominal Aortic Aneurysm by Reducing Inflammation and Extracellular Matrix Degradation. Arterioscler Thromb Vasc Biol 2020;40:2494-507.
36. De Maré A, Maudsley S, Azmi A, et al. Sclerostin as Regulatory Molecule in Vascular Media Calcification and the Bone-Vascular Axis. Toxins (Basel) 2019;11:428.
37. Lin H, Angeli M, Chung KJ, et al. sFRP2 activates Wnt/β-catenin signaling in cardiac fibroblasts: differential roles in cell growth, energy metabolism, and extracellular matrix remodeling. Am J Physiol Cell Physiol 2016;311:C710-9.
38. Frysz M, Gergei I, Scharnagl H, et al. Circulating Sclerostin Levels Are Positively Related to Coronary Artery Disease Severity and Related Risk Factors. J Bone Miner Res 2022;37:273-84.
39. Gay A, Towler DA. Wnt signaling in cardiovascular disease: opportunities and challenges. Curr Opin Lipidol 2017;28:387-96.
40. Bundy K, Boone J, Simpson CL. Wnt Signaling in Vascular Calcification. Front Cardiovasc Med 2021;8:708470.
41. Chen B, Zhao Y, Han D, et al. Wnt1 inhibits vascular smooth muscle cell calcification by promoting ANKH expression. J Mol Cell Cardiol 2019;135:10-21.
42. Hermans KC, Daskalopoulos EP, Blankesteijn WM. Interventions in Wnt signaling as a novel therapeutic approach to improve myocardial infarct healing. Fibrogenesis Tissue Repair 2012;5:16.
43. Daskalopoulos EP, Hermans KC, Janssen BJ, et al. Targeting the Wnt/frizzled signaling pathway after myocardial infarction: a new tool in the therapeutic toolbox? Trends Cardiovasc Med 2013;23:121-7.
44. Cao J, Tsenovoy PL, Thompson EA, et al. Agonists of epoxyeicosatrienoic acids reduce infarct size and ameliorate cardiac dysfunction via activation of HO-1 and Wnt1 canonical pathway. Prostaglandins Other Lipid Mediat 2015;116-117:76-86.
45. Baruah J, Hitzman R, Zhang J, et al. The allosteric glycogen synthase kinase-3 inhibitor NP12 limits myocardial remodeling and promotes angiogenesis in an acute myocardial infarction model. J Biol Chem 2017;292:20785-98.
46. Wang Z, Wang Z, Gao L, et al. miR-222 inhibits cardiac fibrosis in diabetic mice heart via regulating Wnt/β-catenin-mediated endothelium to mesenchymal transition. J Cell Physiol 2020;235:2149-60.
47. Yousefi F, Shabaninejad Z, Vakili S, et al. TGF-β and WNT signaling pathways in cardiac fibrosis: non-coding RNAs come into focus. Cell Commun Signal 2020;18:87.
48. Wang J, Qiu X, Xu T, et al. Sclerostin/Receptor Related Protein 4 and Ginkgo Biloba Extract Alleviates β-Glycerophosphate-Induced Vascular Smooth Muscle Cell Calcification By Inhibiting Wnt/β-Catenin Pathway. Blood Purif 2019;47 Suppl 1:17-23.

(English Language Editor: J. Teoh)

Cite this article as: Zheng S, Wei J, Chen P, Chen F, Yang G. Sclerostin aggravates cardiac remodeling after myocardial infarction by inhibition of Wnt/β-catenin signaling pathway. J Thorac Dis 2022;14(5):1563-1577. doi: 10.21037/jtd-22-473

Supplementary

Table S1 Echocardiographic data

Echocardiographic indicators	Control	Model	SOST-overexpression	sh-SOST
LVEDD, mm	3.45±0.38	4.56±0.54	4.89±0.78	3.91±0.41
LVESD, mm	1.94±0.21	3.56±0.44	3.76±0.39	2.32±0.34
EF, %	76.41±4.53	40.21±5.32	36.75±3.89	58.84±8.76
FS, %	49.83±3.56	21.22±3.16	14.83±1.79	34.43±4.24

LVEDD, left ventricular end-diastolic dimension; LVESD, left ventricular end systolic dimension; EF, ejection fraction; FS, fractional shortening; SOST, sclerostin.

https://dx.doi.org/10.21037/jtd-22-473